Numerical Simulation of Rock Breakage Modes under Confining Pressures in Deep Mining: An Experimental Investigation

Xuefeng Li[1], Shibo Wang[1,*], Reza Malekian[2], Shangqing Hao[3], Zhixiong Li[1, 4]

1 School of Mechanical Engineering, China University of Mining and Technology, Xuzhou 221000, China

2 Department of Electrical, Electronic & Computer Engineering, University of Pretoria, Pretoria 0002, South Africa

3 Shanxi TZ Coal Mine Whole-set Equipment Co., Ltd, Taiyuan 030000, China

4 School of Mechanical and Manufacturing Engineering, UNSW Australia, Sydney 2052, Australia

***Abstract*--The cutting efficiency in underground excavations relies on the optimum parameters of the cutting tool and the cutting process. However, the optimization of the cutting tool design and the cutting process is a challenge and requires knowledge about the tool–rock interaction. This work aims to investigate the tool–rock interaction using a rock cutting mathematical model. The confining pressure was considered in the rock cutting model with conical cutters and the discrete element method (DEM) was adopted to calculate the dynamics of the rock breakage of this model. Graded particle assemblies were created, calibrated and compressed in the horizontal direction with a certain confining pressure. Afterwards, the initiation and propagation of cracks during the rock cutting processes were recorded. A series of small-scale rock cutting tests were also carried out to verify the numerical model. The analysis results demonstrate that (a) the confining pressure induced larger cutting force than that in the unconfined condition, (b) with increase of the confining pressure, the rock failure mode experienced predominantly brittle to predominantly ductile failure, and (c) there was a critical confining pressure/compressive strength ratio of 0.53 when the transition of failure mode occurred.**

Corresponding author: Shibo Wang is with the China University of Mining and Technology, Xuzhou, 221000 China (e-mail: wangshb@cumt.edu.cn).

***Index Terms*--Deep mining, Rock cutting process, Discrete element method, Confining pressure**

I. Introduction

With rapid economic development, the demand and exploitation intensity for resources increases rapidly [1]. The reserve of shallow mineral resources is decreasing and many mines around the world have entered the ‘deep mining’ stage [2]. Taking coal-mining in China as an example, according to the third Chinese national coal resource prediction [3], the total reserve of coal within 2000 m of vertical depth is 5.57 trillion tons. The reserve within 1000 m of vertical depth is 2.86 trillion tons and approximately 70% of this has already been exploited. According to research done in 2004, the coal reserve below 1000 m of vertical depth is 2.95 trillion tons accounting for 53% of the Chinese total coal reserve and there are 1.2 trillion tons in the vertical depth ranging from 1000 to 1500 m. Considering the importance of coal for China, deep mining is an inevitable trend and actually the depth of mining is increasing by 8 to 12 m per year [4].

One of the most important characteristic influencing deep mining machinery is the complex operating environment, which includes: high in-situ stress, temperature, and pressure [5]. As the mining depth increases, nonlinear dynamic mechanical phenomena, such as rock blasting, gas outburst, rock rheology,

and water outburst, etc., occur more frequently and the classic theories become entirely or partially invalid [5]. Many researchers have also found that the confining pressure has a significant influence on the rock mechanical characteristic. Parterson [6] investigated various confining pressures to detect the transition from brittle to ductile failure. Mogi [7] [8] studied the deformation and fracture of rocks by triaxial compressive tests on ten dry rocks. It was found that these rocks showed remarkable elastic hysteresis and a simple rule to define the transition from brittle fracture to ductile failure. However, only a qualitative description was made and a critical index was not given to indicate the failure mode transition.

It is therefore crucial to comprehensively understand the dynamics of rock cutting with confining pressures in deep mining (800 m underground or more) [9] [10] Literature reviews indicate that much research has been done on tool-rock indentation under confining pressure with tunnel boring machine (TBM) cutters or shearer picks. With respect to confined rock indentation, Gnirk and Cheatham [11] carried out a series of indentation tests under confining pressures ranging from 0 to 35 MPa and found that there was a critical confining pressure where the rock exhibited a macroscopic transition from predominantly ductile to predominantly brittle failure mode. Chen and Labuz [12] observed a brittle failure mode with small confinement/compressive strength ratios of 0.1 and 0.06 and a ductile failure mode with the ratio of 0.5. An inclination of the crack propagation was also observed under a small confining pressure by means of the vertical crack test. Innaurato et al. [13] found that the thrust load increased with an increase of the confining pressure by means of indentation tests and the fractures were more evidently directed towards the free edge when the flat-jack pressure was 5 or 10 MPa. Yin et al. [14] concluded, by means of indentation tests with TBM cutters, that there was a critical confining stress level. Below this critical level, the cutting energy increased as the cutting force increased. Otherwise, the rock failure induced by the confining stress required only a small cutting energy and force. Ma et al. [15] carried out indentation tests with TBM cutters and found that the confining pressure increased with an increase of the chipping force and crack angle. Huang and Detournay [16] investigated the effect of confining pressure on the failure mechanism during indentation and found that at the initiation of the primary crack the critical depth of penetration increased with an increase of the lateral confining pressure. Gehring [17] found that in similar rock conditions the disk consumption in deep mining was greater than that in shallow mining during tunnel excavation. The reason for this is the high confining pressure in deep mining. Liu et al. [18] studied the rock breaking and chipping characteristics of TBM cutters under confining stresses by means of theoretical and experimental investigations. It was found that the chips were nearly rectangle shaped and that the height decreased with increasing confining pressure. Indentation tests were also conducted with TBM cutters to investigate the influence of confining stress on the fracture process of soft and hard rocks [19] [20]. Ma, et al. [21] investigated the influence of confining stress on TBM performance in granite by means of full-scale cutting tests. It was found that the normal force increased with increasing confining stress due to the enhancement of the rock resistance strength, while the rolling force decreased gradually with increasing confining stress. Wang Z Q, et al. [22] conducted disc cutter boring process under confining pressures using Rock Failure Process Analysis and found that the vertical cracks were restrained by confining pressures.

Some studies have also been conducted on rock-cutting with conical cutters under confining pressures. Bilgin et al. [23] concluded by means of numerical simulations and small-scale rock cutting tests, that confining pressure dramatically decreases tensile stresses around the cutting groove. For unrelieved cutting, a confining pressure of 1/5 or 1/4 of sample uniaxial compressive strength in magnitude causes an increase of around 60 percent in the cutting

force. For relieved cutting, an increase in the cutting force of around 20 or 30 percent was found. Huang et al. [24] performed numerical simulations of rock cutting with lateral pressure by means of finite element method (FEM) software LS-DYNA3D which is a general explicit nonlinear finite element analysis program. The authors concluded that the cutting force increased with increasing lateral pressure and that the quality and particle size of chips were larger than those in non-lateral pressure conditions. Thus, a better understanding of the effect of confining pressure on rock breakage is necessary during rock cutting by means of a conical cutter.

In this study, a numerical model for rock cutting with confining pressure is established. A commercial discrete element method (DEM)-software called the Particle Flow Code in 2 Dimensions (PFC^{2D}) is used to calculate the dynamics of the model. The advantage of PFC^{2D} is that cracks in particle assembly can be recorded. A series of numerical simulations of rock cutting under different confining pressures is performed to investigate the effect of confining pressure on rock breakage. Furthermore, small-scale rock cutting tests are conducted under lateral confining pressures to validate the effectiveness of the proposed rock cutting model.

II. BASIC THEORY OF DEM

DEM was first used in [25] [26] [27] to model and analyze rock mechanics. The DEM model is discretized into granular elements and interaction between elements only happen at contact points. PFC^{2D} implements DEM by restricting the elements to rigid spherical particles [28]. The interaction of the particles in DEM is regarded as a transient problem. At the contact points, DEM alternates between Newton's second law and the force-displacement law to find the equilibrium state. Newton's second law is used to describe the force-motion relationship and the force-displacement law is used to describe the force-displacement relationship. The force, motion and location of the particles and walls are calculated and updated cycle by cycle. The calculation cycle is shown in Fig. 1.

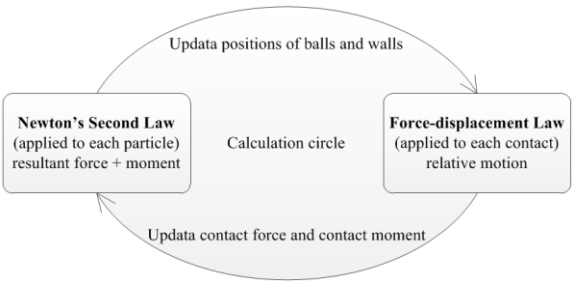

Fig. 1. Calculation cycle in DEM.

With PFC^{2D}, particles are connected together and transmit movement and force to one another through bonds. Bonds are described as gluing two particles together, restricting sliding or rotation [29]. The linear parallel bond contact model is widely used in simulating rock because it can restrict both force and moment between particles. If the strength of the bond exceeds the limitation, the linear parallel bond contact will break down. The initiation and propagation of cracks can be recorded in detail using DEM during the break-down of the linear bonds.

The total force and moment, $\overline{F}_i$ and $\overline{M}_i$, with respect to the parallel bond can be expressed by Fig. 2. The total force $\overline{F}_i$ can be divided into normal and shear force components according to the contact plane. Equation (1) describes their relationship [30].

$$\overline{F}_i = \overline{F}_i^n + \overline{F}_i^s \tag{1}$$

where, $\bar{F}_i^n$ and $\bar{F}_i^s$ are the normal and shear force components, respectively.

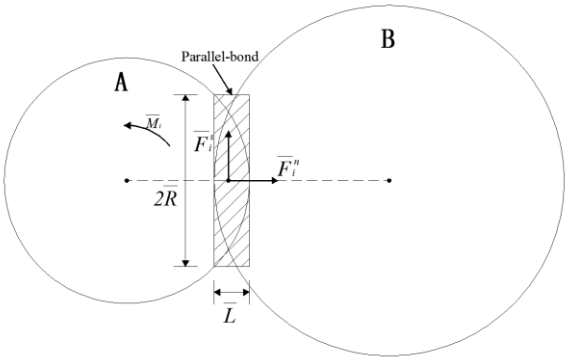

Fig. 2. Parallel bond depicted as a rectangle of cement material [30].

When the bonds are formed, $\overline{F}_i$ and $\overline{M}_i$ are initialized to zero. Each subsequent relative dis-

placement and rotation-increment at the contact points results in an increment of elastic force and moment [30].

$$\bar{F}_i^n = \bar{F}_i^n + \Delta\bar{F}_i^n \tag{2}$$

$$\bar{F}_i^s = \bar{F}_i^s + \Delta\bar{F}_i^s \tag{3}$$

$$\bar{M}_i = \bar{M}_i + \Delta\bar{M}_i \tag{4}$$

$$\Delta\bar{F}_i^n = -k^n A \Delta U_i^n \tag{5}$$

$$\Delta\bar{F}_i^s = -k^s A \Delta U_i^s \tag{6}$$

$$\Delta\bar{M}_i = -k^n I \Delta\theta_i \tag{7}$$

$$\text{with } \Delta U_i = V_i \cdot t\,,\ \ \Delta\theta_i = (\omega_i^B - \omega_i^A)\cdot t\,,$$

$$A = 2\bar{R}\,,\ \ I = \frac{2}{3}\bar{R}^3$$

where Δ is a symbol meaning the increment and ΔU_i is the relative displacement between the bonded particles in one time step and the superscript of n and s represent normal and shear directions, respectively, t is the time step, V_i is the relative velocity between the bonded particles, $\Delta\theta_i$ is the relative rotation angle between the bonded particles, ω^A and ω^B are angular velocities of the bonded particles, A is the area of the bond disk, I is the moment of inertia of the disk cross-section about an axis through the contact point and in the direction of $\Delta\theta_i$, $\bar{R}$ is the parallel-bond radius, k^n and k^s are the normal and shear contact stiffness, respectively.

III. THE PROPOSED ROCK CUTTING MODEL

To investigate the influence of confining pressure, rock cutting tests were simulated under 0, 2, 5, 10 and 15 MPa of confining pressure with a cutting depth of 3 mm and cutting distance of 96 mm using a conical cutter. For this purpose, graded particle assemblies were created and calibrated according to uniaxial compressive strength (UCS) tests and Brazilian tensile strength (BTS) tests on a synthetic rock sample in the laboratory. The synthetic rock sample used in the laboratory is a mixture of cement and sand with a mass ratio of 3:1 referring to Tu [31]. The UCS, BTS, elastic modulus and Poisson's ratio properties of the synthetic rock are 28 MPa, 2.5 MPa, 18 GPa and 0.24, respectively obtained by UCS and BTS tests in laboratory.

The variation of cutting forces on the conical cutter was recorded and its mean peak was obtained in the laboratory test. In addition, the initialization and propagation of cracks were recorded to study the mechanics of the rock breakage.

A. Graded Rock Specimens

The linear contact model was used to establish the rock specimens under confining pressure in PFC^{2D}. The rock sample is 120 mm in length and 60 mm in height. In order to ensure the accuracy and decrease calculation time, the particle assembly is graded into two levels with particle radii increasing downwards from the upper surface. The heights of layer 1 and layer 2 are 12 mm and 48 mm, respectively. The interface layer (as depicted in Fig. 3) ensures the homogeneity in the interface between layer 1 and layer 2. To ensure accuracy [29], at least 10 particles should interact with the cutter during cutting, with a cutting depth of 3 mm. The radii of the particles of layer 1, layer 2 and the interface range from 0.1 to 0.3 mm, 0.3 to 0.5 mm and 0.1 to 0.5 mm, respectively. Particle radius is one of the factors determining the macro properties of rock specimen, so it's essential to calibrate micro parameters for layer 1, layer 2 and the interface respectively. The rock model included approximately 24578 particles. Fig. 4 shows the particle size distribution of layer 1 and layer 2. The radii of particles were drawn from uniform distribution throughout the model domain.

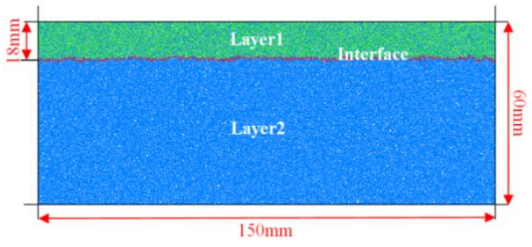

Fig. 3. Graded rock specimen

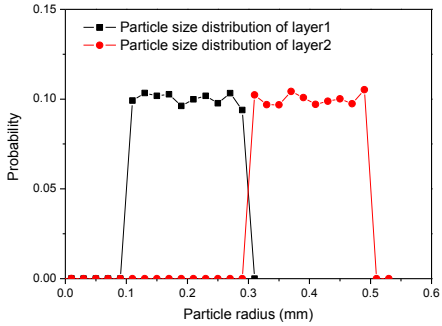

Fig. 4. Particle size distribution of rock sample

B. *Model Calibration*

The linear parallel bond model was used in modeling the synthetic rock sample, which can transmit both force and moment between particles. The micro parameters of the parallel bond particle model defined in PFC^{2D} [30] are particle radius (r), particle elastic modulus (E'), particle normal-to-shear stiffness ratio (k'), parallel bond elastic modulus ($\overline{E}$), parallel bond normal-to-shear stiffness ratio ($\overline{k}$), parallel bond tensile strength ($\overline{\sigma_c}$), parallel bond cohesion strength ($\overline{c}$) and porosity (n). In this study, in order to reduce the number of independent parameters, the particle elastic modulus and particle stiffness ratio are equal to the bond elastic modulus and bond stiffness ratio respectively. The porosity is also set to a constant of 0.1, in order to model a density rock specimen. Thus, the independent variables are [$\overline{E}$, $\overline{k}$, $\overline{\sigma_c}$, $\overline{c}$, r].

Since the relationship between micro properties and the macro response of particle assembly is not certain, it is repetitive work to get the appropriate micro properties. The micro properties were calibrated by modeling UCS tests and BTS tests in PFC^{2D}. The macro properties of rock are described by the UCS (σ_c), elastic modulus (E), Poisson's ratio (μ) obtained by UCS test and BTS (σ_t) obtained by BTS test. A standard specimen was made for the UCS test with dimensions 50 ×100 mm and a circular disk specimen for the BTS test was cut out from a square particle assembly with dimensions 50 ×50 mm [32]. These were created according to the specimen-genesis procedure mentioned by Potyondy and Cundall [33]. Particle assembles for UCS and BTS tests are shown in Fig. 5.

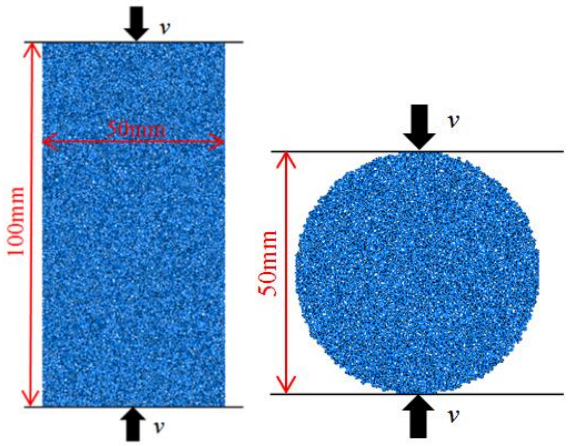

(a) (b)

Fig. 5. Models for (a) UCS and (b) BTS tests.

Fortunately, there are empirical rules, as stated in [34], for calibration:

1) Elastic Modulus is matched firstly by setting the bond strength to a high value and varying the particle elastic modulus and parallel bond elastic modulus.

2) Poisson's ratio is matched by varying the particle normal-to-shear stiffness ratio.

3) The UCS is matched by varying the parallel bond tensile and shear strength.

According to the rules above, the micro properties of the rock specimen for each layer was acquired after a series of calibration. Simulations of the mechanical properties for each layer of the rock specimen were repeated at least three times by changing the random number which determines the distribution of the size and position of the particles. The results of the calibration are summarized in Table 1 and Table 2. The elastic modulus, UCS, and Poisson's ratio were reproduced very well. The BTS was a little larger since the parallel bond model in PFC produces unrealistically low ratios of compressive to tensile strength [33]. The cracks of the rock were reproduced very well in the simulation tests in comparison with the laboratory tests, as shown in Fig. 6.

TABLE 1. Micro parameters of particle assembly

Micro parameters	Layer 1	Interface	Layer 2
Particle radius (r)	0.1-0.3 mm	0.1-0.5 mm	0.3-0.5 mm

Bond elastic modulus ($\overline{E}$)	10 GPa	10.5 GPa	9.8 GPa
Bond stiffness ratio (k)	2.1	2.1	2.1
Bond tensile strength ($\overline{\sigma_c}$)	12.05 MPa	12.6 MPa	11.6 MPa
Bond shear strength ($\overline{\tau_s}$)	12.05 MPa	12.6 MPa	11.6 MPa
Particle elastic modulus (E')	10 GPa	10.6 GPa	9.8 GPa
Particle stiffness ratio (k')	2.1	2.1	2.1

TABLE 2. Macro properties of rock specimen.

Property	Laboratory test	Simulation		
		Layer 1	Interface	Layer 2
UCS (MPa)	28.01±3.79	28.60±1.52	27.90±0.67	28.10±0.98
E (GPa)	18.27±3.25	18.21±0.03	18.21±0.09	18.37±0.18
μ	0.2418 ±0.0287	0.250 ±0.003	0.251 ±0.004	0.247 ±0.012
BTS (MPa)	2.55±1.02	4.07±0.182	4.07±0.346	4.25±0.233

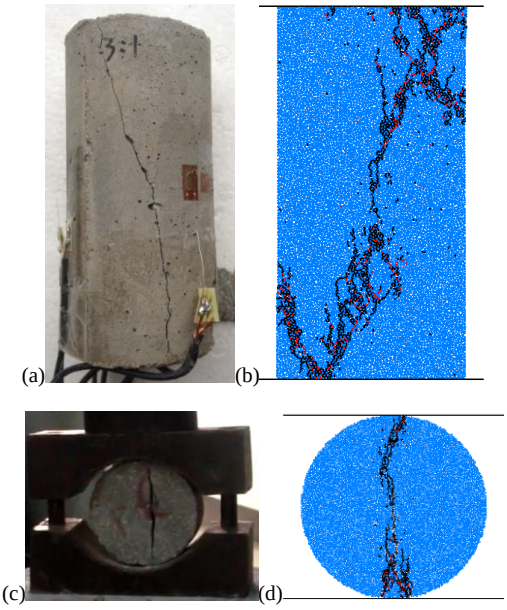

Fig. 6. Cracks of rock in the laboratory and simulation (layer 1) tests. (a) Cracks of rock sample for UCS tests in a laboratory and (b) Cracks of rock sample for UCS tests with simulation. (c) Cracks of rock sample for BTS tests in a laboratory and (d) Cracks of rock sample for BTS tests with simulation.

Axial stress-axial strain curves for the simulation and laboratory tests are shown in Fig. 7. According to this figure, there is a significant difference between the simulation and laboratory tests with regards to pre-peak properties. There is a concave upward stage called 'compaction stage' in the laboratory test at the beginning of compression, because the rock sample used in the laboratory test contains micro-fractures or pores inside [35]. However, the rock specimen used in the simulation is homogeneous and isotropic with certain porosity. The similarity in properties of stages after compaction and the pro-peak properties of the simulation and laboratory tests indicate that the failure limit and failure mode are almost the same. The stress-strain curves decrease rapidly after the peak stress, suggesting that the failure mode of the rock is brittle.

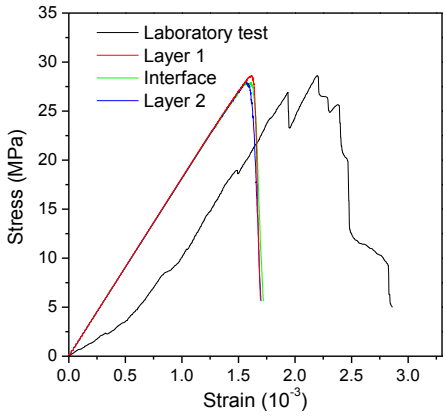

Fig. 7. Axial stress-axial strain curves of the simulation and laboratory tests.

C. Modeling of the Rock Cutting under Confining Pressure

The micro parameters of the parallel bond contact model obtained above were applied to the rock specimen. Since stress on a wall cannot be applied directly in PFC，servo-controlled velocities were applied to the lateral walls to provide confining pressure. A servo-control algorithm was employed to adjust the magnitude and orientation of the velocities of the lateral walls implemented via a FISH (an embedded programming language in PFC) function described in (8) and (9) [28]

$$\dot{u}^{(w)} = G(\sigma^{cur} - \sigma^{tar}) = G \cdot \Delta\sigma \qquad (8)$$

$$G = \frac{\alpha \cdot S}{k_n' N_c t} \tag{9}$$

where $\dot{u}^{(w)}$ is the velocity of the lateral walls, σ^{cur} and σ^{tar} are the current stress and the target stress respectively acting on the lateral walls, $\Delta\sigma$ is the difference between σ^{cur} and σ^{tar}, G is the velocity gain, α is the relaxation factor used to insure the stability, S is the area of the wall, k'_n is the average stiffness of contacts on the wall, N_c is the number of contacts on the wall, t is the time step.

Firstly, the specimen was compacted to a required confining pressure vertically and horizontally. Rock samples were compacted for subsequent rock-cutting simulation under confining pressures of 0, 2, 5, 10 and 15 MPa. Fig. 8 shows the variations of the confining pressure versus the time step during compaction using the servo-control algorithm FISH function. It can be seen that the loading speed decreases until the confining pressure increases to the target confining pressure. The volume strain of the rock specimen after compaction was calculated via (10) and results are summarized in Table 3.

$$\varepsilon_v = \frac{V_0 - V_c}{V_0} \tag{10}$$

where ε_v is volume strain, V_0 is the initial volume of rock specimen, V_c is the volume of the rock specimen after compaction.

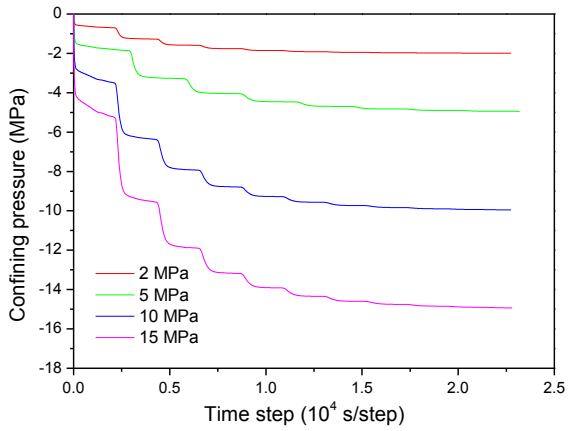

Fig. 8. Variations of the confining pressure versus the time step during compaction.

After being compacted, the upward wall was deleted representing the free surface and a conical cutter shaped wall was imported into the left side of the rock with a cutting depth of 3 mm. The conical cutter shaped wall has a tip angle of 55 ° and a diameter of 19 mm which was treated as rigid without wear. The lateral walls were used to provide the confining pressure during the cutting process. Fig. 9 shows the schematic of the rock cutting model under confining pressure.

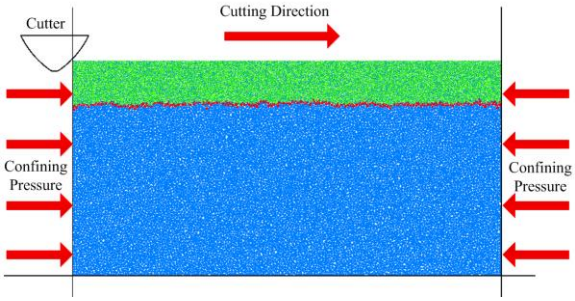

Fig. 9. Rock cutting model under confining pressure.

IV. LABORATORY TESTS FOR ROCK CUTTING DUNER CONFINING PRESSURE

Small-scale cutting tests were carried out with the conical cutters under confining pressure. The schematic of the small-scale rock cutting rig are shown in Fig. 10a. The cutter head used here is an alloy head of the real conical cutter with a tip angle of 55 ° and a diameter of 19 mm. The dimensions of the synthetic rock sample are 150 × 150 × 65 mm. Fig. 10b shows the rock sample fixture which fixes the rock sample and provides the confining pressure by screwing the nut.

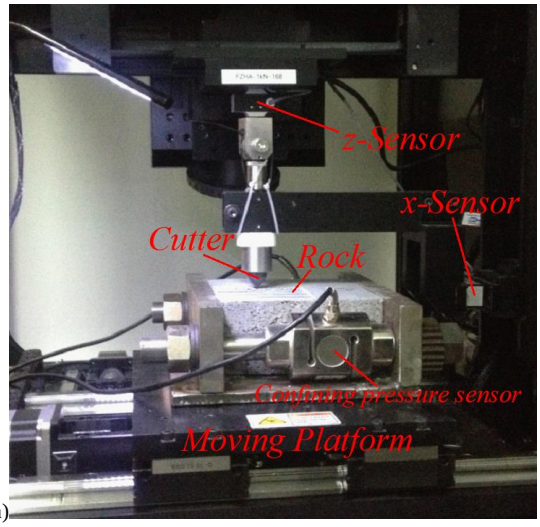

(a)

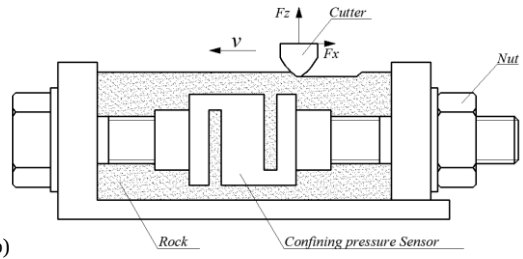

(b)

Fig. 10. (a) A schematic of the small-scale cutting rig and (b) the rock sample fixture.

Limited by the measuring range of force sensor and space of the test rig, the cutting process was performed with a cutting speed of 6 mm/s, a cutting distance of 120 mm and a cutting depth of 3 mm under confining pressure of 0 and 2 MPa. During the cutting process two components of the force (cutting force and normal force) were recorded at a frequency of a 1000 Hz and plotted versus the cutting displacement as shown in Fig. 11. In these figures, random vibrations of the curve can be observed which are induced by the formation of chips. It can be seen that the cutting force under confining pressure is much larger than that without confining pressure.

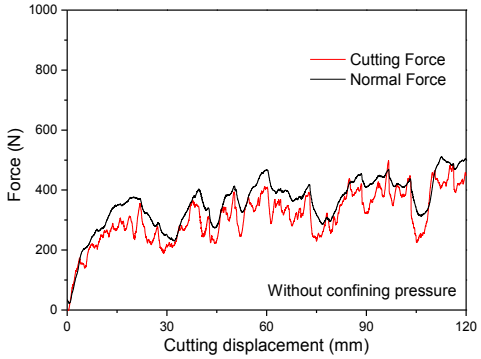

(a)

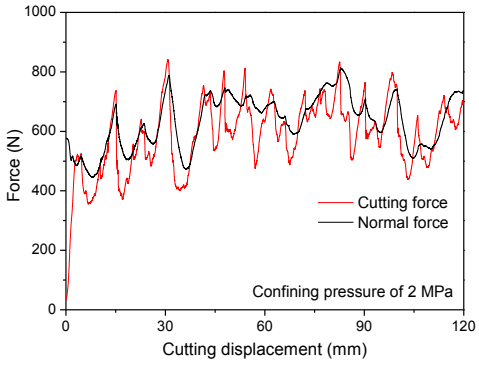

(b)

Fig. 11. Variations of forces under confining pressures of (a) 0 and (b) 2 MPa.

V. SIMULATIONS OF ROCK CUTTING UNDER CONFINING PRESSURE

Numerical tests were conducted using the graded particle assembly mentioned above under different confining pressures of 0, 2, 5, 10 and 15 MPa. In order to insure the reliability of the result, the cutting simulation was repeated three times under each confining pressure on different rock specimens which were generated with different random numbers. The random number determines the distribution of the size and position of the particles. Since it would take too much time using the real cutting speed of 6 mm/s, a cutting speed of 6 m/s and cutting distance of 96 mm was applied. The time-step is approximately 2.3 $\times 10^{-8}$ s/step, so that the displacement of the cutter is approximately 1.38×10^{-4} mm in each step. Compared with the radius of the smallest particle of 0.1 mm, the displacement of the cutter in each step is small enough to guarantee particle assembly in a quasi-static equilibrium state. During the cutting process, the normal and cutting forces acting on the cutter were recorded with the step interval of 10 steps. In Fig. 12 the variations of the confining pressure during cutting under different confining conditions is shown. Considering the sensitivity of the servo-control algorithm, the confining pressure was steady save for a few deviations in the curves. The variations of the cutting and normal forces versus the cutting displacement under the confining pressure of 2 MPa are shown in Fig. 13. The mean force and mean peak force were obtained from historic data.

The results are summarized in Table 3 and the mean forces and the mean peak forces are plotted versus confining pressures in Fig. 14. The results show that as confining pressure increases, the mean forces and mean peak forces increase dramatically. The increase of volume strain (ε_v) indicates that the rock specimen is denser after being compacted under higher confining pressure which may be the reason for the increase of the cutting force.

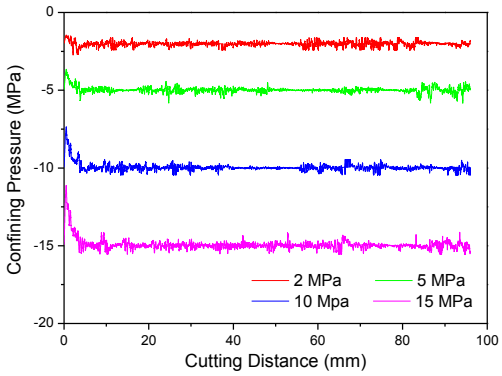

Fig. 12. The variations of the confining pressure during cutting under different confining conditions.

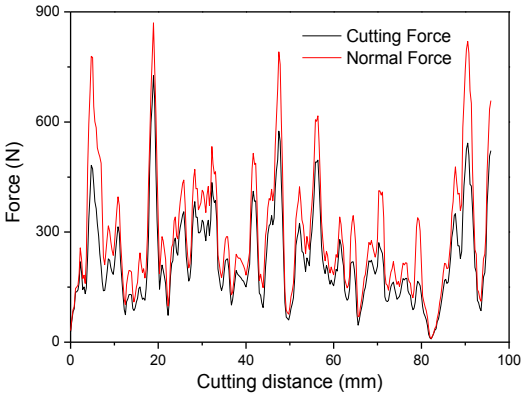

Fig. 13. The variations of the forces versus the cutting distance under confining pressure of 2 MPa.

TABLE 3. Summary of the rock cutting test results under confining pressure at 3mm depth of cut

Confining pressure(MPa)	*FC*±*sd* (N)	*FN*±*sd* (N)	*FC'*±*sd* (N)	*FN'* ±*sd* (N)	ε_v (10^{-4})
0	191.7±158.1	253.3±215.3	330.8±108.4	436.6±154.6	0
2	221.5±176.4	301.7±277.4	388.7±140.4	579.1±296.7	1.67
5	312.9±333.8	482.2±412.1	573.7±267.6	765.5±356.6	4.18
10	323.6±496.4	540.8±629.5	575.9±391.4	805.6±556.9	8.36
15	375.5±360.9	667.8±550.4	718.0±302.1	1055.6±475.4	12.54

FC: mean cutting force, *FN*: mean normal force, *FC'*: mean peak cutting force, *FN'*: mean peak normal force, ε_v: volume strain of rock specimen after compacted, ±*sd*: standard deviation.

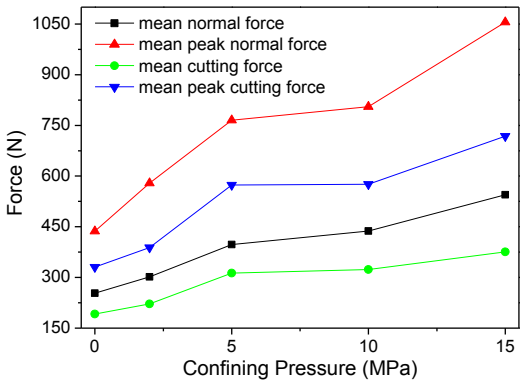

Fig. 14. Relationship between the cutting forces and the confining pressure.

During simulation, the initiation and propagation of cracks, indicated by broken bonds, was monitored. When the contact force exceeds the shear or tensile strength, the parallel bond fails and a fracture is generated. Fig. 15-Fig. 19 show the initiation and propagation of cracks during cutting with confining pressures of 0, 2, 5, 10 and 15 MPa, respectively. These figures suggest that shear fractures (in green) are dominant at initiation of the cracks while the propagation of cracks are induced by tensile fractures (in black) which is in accordance with the maximum tensile stress criterion proposed by Evans [36].

From these figures, it is shown that the confin-

ing pressure has a significant influence on the propagating orientation and length of the cracks. The mechanism of the initialization of the cracks and chip formation are similar under different confining pressures. Firstly, shear fractures were formed beneath the cutter and particles connected to the cutter separated from the rock sample as powder. As the cutter advanced, tensile fractures increased and coalesced to form macro-cracks. Macro-cracks are divided into vertical and horizontal cracks and the horizontal cracks propagate to the free surface to induce chips. The main difference between the different confining conditions is the propagating orientation and length of the primary cracks. For unconfined conditions, vertical and horizontal propagation of the cracks were observed. The vertical cracks are almost perpendicular to the free surface of the rock sample and propagate to a certain depth. The horizontal cracks propagate to the free surface and induce chips. As the confining pressure increased, vertical cracks tilted and were restricted, while horizontal cracks induced chips until the confining pressure was 15 MPa. The crack propagation and chip generation suggest that the failure mode of the rock is brittle. When the confining pressure was 15 MPa, propagation of all cracks was restricted and the ductile failure mode of rock was observed. It can be concluded that 15 MPa is the critical confining pressure at which the failure mode of rock translates from brittle to ductile. A similar conclusion was also obtained by Gnirk and Cheatham [11] and Chen and Labuz [12]. Hence, the critical confining pressure/compressive strength ratio is 0.53 for the synthetic rock used in this study.

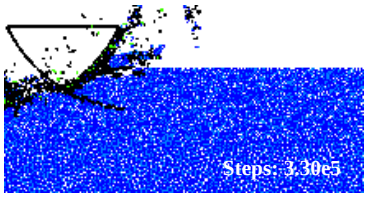

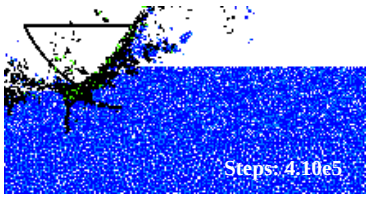

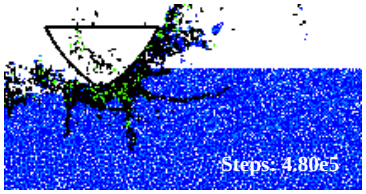

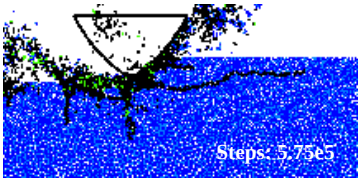

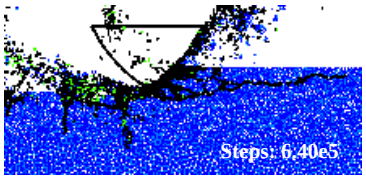

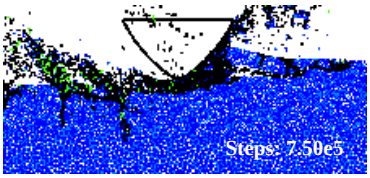

Fig. 15. Initiation and propagation of cracks with a confining pressure of 0 MPa.

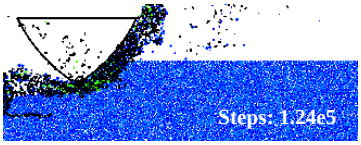

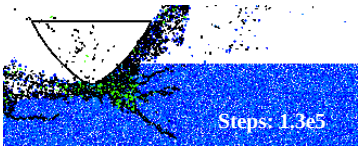

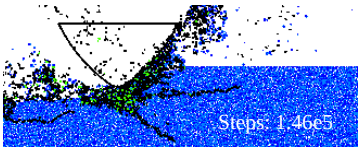

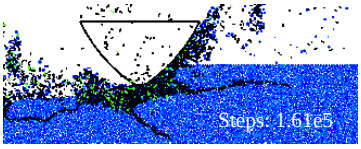

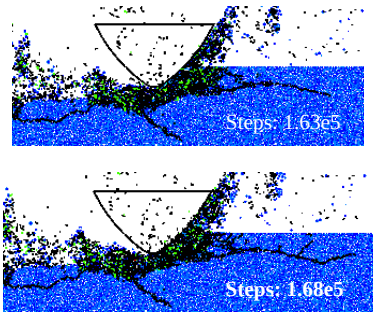

Fig. 16. Initiation and propagation of cracks with a confining pressure of 2 MPa.

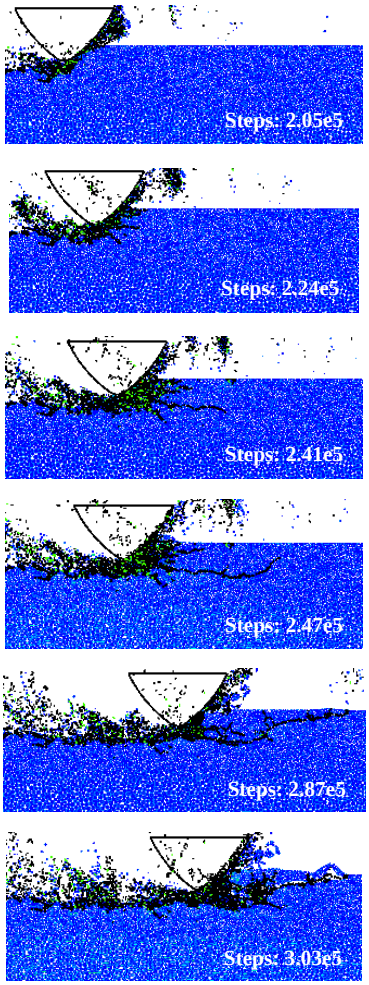

Fig. 17. Initiation and propagation of cracks with a confining pressure of 5 MPa.

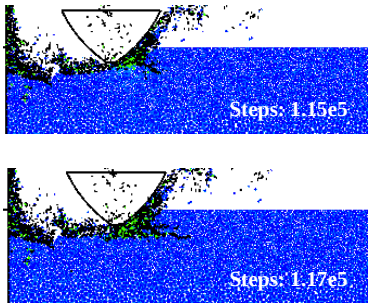

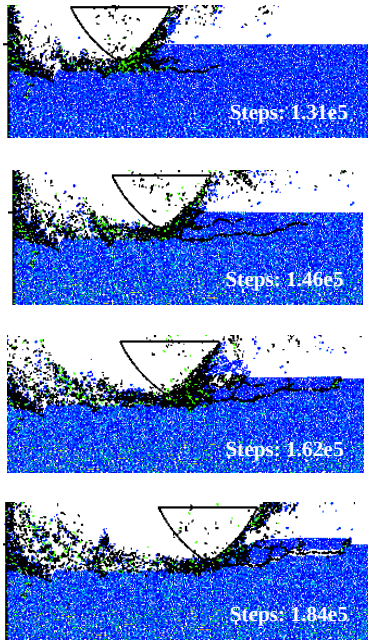

Fig. 18. Initiation and propagation of cracks with a confining pressure of 10 MPa.

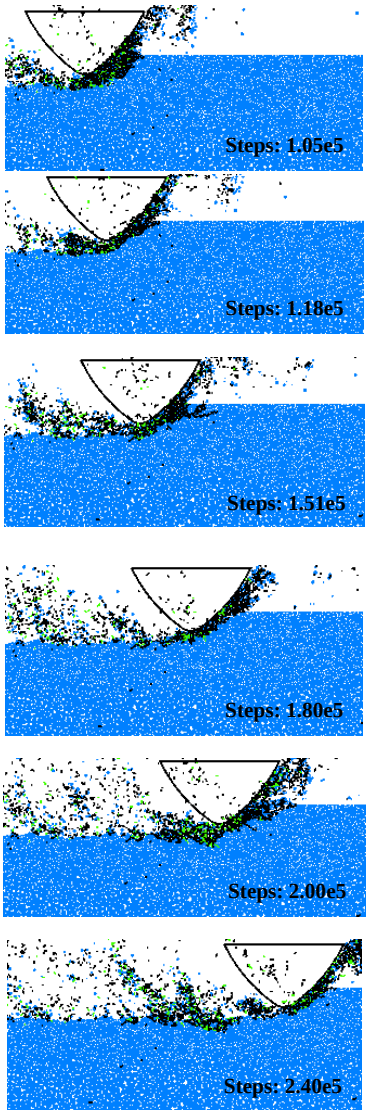

Fig. 19. Initiation and propagation of cracks with confining pressure of 15 MPa.

VI. Comparison of Simulation and Laboratory Results

The comparison of the mean forces and standard deviations obtained from the laboratory and simulation tests are shown in Fig. 20. It shows that the DEM simulation gives a good prediction of the changes of forces while confining pressure increases. The reason for the distinction in value of the mean force and standard deviation is the disadvantage of the PFC^{2D} [37]. In two dimensions, the cutter is regarded as a cone-shaped plate with unit thickness, while the real cutter is conical-shaped in three dimensions [39]. However, it is more vivid and intuitive to observe the initialization and propagation of cracks in PFC^{2D} for small-scale tests since fractures are presented by segments in PFC^{2D} and disks in Particle Flow Code in 3 dimensions (PFC^{3D}). The propagation of macro-cracks can be represented as coalesced segments in PFC^{2D} while disks are isolated in PFC^{3D}. However, in order to predict the cutting force [40] more accurately, PFC^{3D} should be employed in future work.

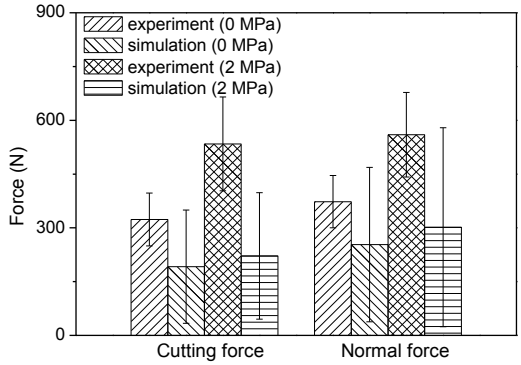

Fig. 20. Comparison of mean forces and standard deviations obtained from the laboratory and simulation tests.

VII. Conclusion

The DEM simulation can provide valuable information during cutting. In this paper, a 2D graded particle assembly was generated and a series of rock cutting numerical simulations under different confining pressures was carried out. During the cutting processes, the cutting and normal forces were recorded. The initialization and propagation of cracks during the rock cutting were dynamically displayed. The results of the laboratory rock cutting tests were also presented.

The results show that the confining pressure has significant influence on the cutting force and propagation of cracks. Larger mean forces and mean peak forces were required in higher confining pressure conditions. As confining pressure increased, the propagation of the tensile crack was restricted which induced the transition of the rock failure mode from predominantly brittle failure to predominantly ductile failure. The critical confining pressure/compressive strength ratio of the failure mode transition for this synthetic rock was found to be 0.53.

Additionally, reasonable agreements of the force variation trend were obtained between the simulation and experimental tests which verified the validity of the DEM rock cutting model. However, due to the limitation of the laboratory equipment, the tests under confining pressure higher than 2 MPa were not conducted. In future research work, higher confining pressure and different types of rock will be taken into consideration and the influence of rock properties on the critical confining pressure index will be investigated.

Acknowledgements

This research was supported by the National Basic Research Program of China (2014CB046301), the China University of Mining and Technology Research Fund (2013ZDP05), the Key Program of Shanxi Coal Basic (MJ2014-05) and the Science and Technology Project of Jiangsu Province (BK20140051), National Research Foundation (NRF), South Africa (IFR160118156967).

References

[1] Y. Jiang, H. Zhu, Z. Li, Z. Peng, "The nonlinear dynamics response of cracked gear system in a coal cutter taking environmental multi-frequency excitation forces into consideration," *NODY*, vol. 84, no. 1, pp. 203–222, 2016.

[2] Z. Li, X. Yan, X. Wang, Z. Peng, "Detection of gear cracks

in a complex gearbox of wind turbines using supervised bounded component analysis of vibration signals collected from multi-channel sensors," *J SOUND VIB*, vol. 371, pp. 406–433, 2016.

[3] J. Mao, H. Xu *Prediction and evaluation of Chinese coal resources*. Beijing: Science Press, 1999.

[4] M. C. He, "Rock mechanics Situation and Prospects of deep mining engineering," in *Eighth Rock Mechanics and Engineering Conference Proceedings*. Beijing: Science Press, 2004.

[5] M. C. He, "Conception system of deep and evaluation index for deep engineering," in *ISRM of Conf*, International Society for Rock Mechanics, 2005.

[6] M. S. Paterson, "Experimental deformation and faulting in Wombeyan marble," *GEOL SOC AM BULL*, vol. 69, no. 4, pp. 465-476, 1958.

[7] K. Mogi, "Deformation and Fracture of Rocks under Confining Pressure (2): Elasticity and Plasticity of Some Rocks," *Bulletin of the Earthquake Research Institute*, vol. 43, pp. 349-379, 1965.

[8] K. Mogi, "Pressure Dependence of Rock Strength and Transition from Brittle Fracture to Ductile Flow," *Bulletin of the Earthquake Research Institute*, vol. 44, pp. 215-232, 1966.

[9] Y. Jiang, H. Zhu, Z. Li, "A new compound faults detection method for rolling bearings based on empirical wavelet transform and chaotic oscillator," *CHAOS SOLITON FRACT*, vol. 89, pp. 8-19, 2016.

[10] M. C. He, H. P. Xie, S P Peng, et al, "Researches of deep mining rock mechanics," *CJRME*, vol. 24, no. 16, pp. 2803-2813, 2005.

[11] P. F. Gnirk, J. Cheatham, "An experimental study of single bit-tooth penetration into dry rock at confining pressures 0 to 5,000 psi," *Soc Petrol Eng J*, vol. 5, no. 2. pp. 117-130, 1965.

[12] L. H. Chen, J. F. Labuz, "Indentation of rock by wedge-shaped tools," *INT J ROCK MECH MIN*, vol. 43, no. 7, pp. 1023-1033, 2006.

[13] N. Innaurato, C. Oggeri, P. P. Oreste, et al, "Experimental and numerical studies on rock breaking with TBM tools under high stress confinement," *ROCK MECH ROCK ENG*, vol. 40, no. 5, pp. 429-451, 2007.

[14] L. J. Yin, Q. M. Gong, H. S. Ma, et al, "Use of indentation tests to study the influence of confining stress on rock fragmentation by a TBM cutter," *INT J ROCK MECH MIN*, vol. 72, pp. 261-276, 2014.

[15] H. Ma, L. Yin, H. Ji, "Numerical study of the effect of confining stress on rock fragmentation by TBM cutters," *INT J ROCK MECH MIN*, vol. 48, no. 6, pp. 1021-1033, 2011.

[16] H. Huang, E. Detournay, "Discrete element modeling of tool - rock interaction II: rock indentation," *INT J NUMER ANAL MET*, vol. 37, no. 13, pp. 1930-1947, 2013.

[17] K. H Gehring, "Design criteria for TBM's with respect to real rock pressure," presented at Tunnel boring machines—trends in design & construction of mechanized tunnelling, International lecture series TBM tunnelling trend of Conf. Hagenberg, AA Balkema, Rotterdam, pp. 43-53, 1996.

[18] J. Liu, P. Cao, K. Li, "A study on isotropic rock breaking with TBM cutters under different confining stresses," *Geotechnical and Geological Engineering*, vol. 33, no. 6, pp. 1379-1394, 2015.

[19] J. Liu, P. Cao, J. Liu, et al, "Influence of confining stress on fracture characteristics and cutting efficiency of TBM cutters conducted on soft and hard rock," *J CENT SOUTH UNIV T*, vol. 22, pp. 1947-1955, 2015.

[20] J. Liu, P. Cao. "Study on Rock Fracture with TBM Cutter under Different Confining Stresses," *IGJ*, vol. 46, no. 1, pp. 104-114, 2016.

[21] H. Ma, Q. Gong, J. Wang, et al, "Study on the influence of confining stress on TBM performance in granite rock by linear cutting test," *TUNN UNDERGR SP TECH*, vol. 57, pp. 145-150, 2016.

[22] Z. Q. Wang, et al. "Cutting simulation and test based on different rock parameters." IEEE International Conference on Information and Automation IEEE, pp:735-740, 2013

[23] N. Bilgin, H. Tuncdemir, C. Balci, et al, "A model to predict the performance of tunneling machines under stressed conditions" in *Proceedings of the AITES-ITA 2000 World Tunnel Congress*, Johannesburg, Republic of South Africa, 2000, pp. 13-18.

[24] J. Huang, Y. Zhang, L. Zhu, T. Wang, "Numerical simulation of rock cutting in deep mining conditions," *INT J ROCK MECH MIN*, vol. 84, pp. 80-86, 2016

[25] P. A. Cundall. "A computer model for simulating progressive large scale movements in blocky rock systems," in *Proceedings of the Symposium of the International Society*

of Rock Mechanics, Nancy, France, 1971.

[26] P. A. Cundall, O. D. L. Strack. “A discrete numerical model for granular assemblies,” *GEOTECHNIQUE*, vol. 29, no. 1, pp. 47-65, 1979.

[27] D. O. Potyondy. “The bonded-particle model as a tool for rock mechanics research and application: current trends and future directions,” *Geosystem Engineering*, vol. 17, no. 6, pp. 342-369, 2014

[28] *PFC2D/3D (Particle Flow Code in2/3 Dimensions) Version 3.0*, Itasca Consulting Group Inc., Minneapolis, MN: ICG; 2004.

[29] O. Su, N. A. Akcin. “Numerical simulation of rock cutting using the discrete element method,” *INT J ROCK MECH MIN*, vol. 48, no. 3, pp. 434-442, 2011.

[30] *PFC2D/3D (Particle Flow Code in2/3 Dimensions) Version 5.0*, Itasca Consulting Group Inc., Minneapolis, MN: ICG; 2014.

[31] S H TU, et al., “*Experimental methods and measuring technology of rock stratum controlling*”. Xu Zhou, China: CUMT Press, 2010, pp. 65-76.

[32] *Standard for Tests Method of Engineering Rock Massa*, GB/T 50266-99, 1999.

[33] D. O. Potyondy, P. A. Cundall, “A bonded-particle model for rock,” *INT J ROCK MECH MIN*, vol. 41, no. 8, pp. 1329-1364, 2004.

[34] S. T. Lei, P. Kaitkay. Distinct element modeling of rock cutting under hydrostatic pressure. Key Engineering Materials, 2003, 250: 110-117.

[35] M. G. Qian, T. C. Liu, *Introduction and control of mine pressure*, Beijing: Coal Industry Press, 1991, pp. 18-19.

[36] I. Evans. “Basic mechanics of the point-attack pick,” *Colliery Guardian*, vol. 232, pp. 189-193, 1984.

[37] J. Rojek, E. Oñate, C. Labra, et al, “Discrete element simulation of rock cutting,” *INT J ROCK MECH MIN*, vol. 48, no. 6, pp. 996-1010, 2011.

[38] Valdo Henriques, Reza Malekian, "Mine Safety System Using Wireless Sensor Network", IEEE Access, Vol.4, pp. 3511-3521, 2016.

[39] Xiangjun Jin, Jie Shao, Xin Zhang, Wenwei An, Reza Malekian, "Modeling of nonlinear system based on deep learning framework", Nonlinear Dynamics, Springer, Vol.84, No. 3, pp.1327-1340, 2016.

[40] Reza Malekian, Dijana Capeska Bogatinoska, Aleksandar Karadimce, Jasna Trengoska, William A. Nyako, "A Novel Smart ECO model for Energy Consumption Optimization", 2015, Elektronika ir Elektrotechnika, Vol. 21, No.6, pp.75-80, 2015